Molecular Dynamics of Poly(L-lysine) Dendrimers with Naphthalene Disulfonate Caps

Benjamin P. Roberts,[†] Martin J. Scanlon,[†] Guy Y. Krippner,[‡] and David K. Chalmers*[,†]

Medicinal Chemistry and Drug Action, Monash Institute of Pharmaceutical Sciences, 381 Royal Parade, Parkville, Victoria 3052, Australia, and Verva Pharmaceuticals Ltd., P.O. Box 1069, Grovedale, Victoria 3216, Australia

Received September 22, 2008; Revised Manuscript Received December 17, 2008

ABSTRACT: We have used atomistic molecular dynamics simulations to study the molecular-scale structure of poly(L-lysine) dendrimers homogeneously functionalized with naphthalene disulfonate caps from the first generation to the sixth generation. These dendrimers behave as typical dendrimers in poor solvent. As the generation number increases, there is a change from small molecule behavior to more polymer-like behavior. The first- and second-generation dendrimers, behaving as small molecules, are flexible, aspherical, and exposed to the environment, and their caps cluster together. Third- and fourth-generation dendrimers exhibit a transition toward polymeric behavior. The fifth- and sixth-generation dendrimers are large, essentially spherical globules, with a dense core, an irregular and highly grooved surface, and caps which are evenly distributed. Cap−cap interaction in all generations is favorable and is characterized by face-to-face naphthalene stacking.

Introduction

Poly(L-lysine) (PLL) dendrimers are a well-established family of dendrimers, first prepared in the early 1980s.[1,2] Though less commonly reported than the poly(amido amine) (PAMAM) dendrimers,[3] the poly(propylene imine) (PPI) dendrimers,[4] or the poly(benzyl ether) dendrimers,[5−7] they show potential in various biological applications, such as gene delivery agents,[8−10] drug carriers,[11,12] peptide antigens,[13,14] vaccines,[15,16] and antimicrobial agents.[17−22] Their key characteristics are flexibility and asymmetry. Dendrimers such as PAMAM or PPI are symmetric in the sense that all chain termini are connected to the core in a topologically identical fashion. By contrast, in a PLL dendrimer, all chain termini are topologically different, so that, for example, some caps are connected to the core through much shorter tethers than others.

A detailed understanding of the structure of PLL dendrimers is necessary if optimized PLL dendrimers are to be designed, but comprehensive characterization of dendrimers has proven to be very difficult. Caminade et al. have discussed efforts in this area in a 2005 review.[23] An alternative approach to physical experiments is computer simulation, which is widely recognized as a method of studying and predicting dendrimer structure. A pioneering theoretical study of dendrimers was carried out as early as 1983 by de Gennes and Hervet.[24] This study predicted that the atom density should increase toward the periphery of the molecule in the so-called "dense shell" model. More recent studies, beginning with that of Lescanec and Muthukumar in 1990,[25] have tended to reject the dense-shell model in favor of a dense-core model, in which the atom density is greatest in the center of the dendrimer and decreases toward the periphery. Although dendrimer simulation is a significant area of research, with several new studies reported annually, PLL dendrimers have scarcely been studied by computer simulation. We are aware of only three such studies. Arai et al.[26] performed an energy calculation on a first-generation PLL dendrimer with a fullerene core and porphyrin caps. Short simulations, up to 200 ps, have been carried out on specific PLL dendrimers by Cattani-Scholz et al.[27] and Al-Jamal et al.[28] There is considerable scope for fuller computational treatments of PLL dendrimers.

In the present work, we study a series of capped PLL dendrimers using molecular dynamics (MD) simulations. The caps play an important role in determining the molecular-scale structure of the dendrimer as well as other biologically relevant properties such as solubility and toxicity.[29] For example, dendrimers with cationic surface groups are almost always toxic, while dendrimers with anionic surface groups are much less so.[30] Here, we present MD simulations of a series of PLL dendrimers with naphthalene disulfonate caps. These caps are notable for giving dendrimers, including PLL, antiviral activity;[20,21] in particular, the fourth-generation dendrimer in this family is presently undergoing clinical trials as VivaGel, a topical microbicide.[31] MD simulations reveal new information about the molecular-scale structures of dendrimers in this family, from the first to the sixth generation.

Methods

Dendrimer Construction. Dendrimers were built using the program Starmaker which is part of Silico,[32] our suite of molecular data processing and analysis scripts. Starmaker is a flexible program which can be used to construct a wide variety of dendrimers, including heterogeneously functionalized (variegated) dendrimers. Starmaker constructs dendrimers from a core by repeated addition of generations of monomers. As each monomer unit is added, a stochastic search is used to attain an extended conformation for the monomer, while leaving the remainder of the dendrimer intact. This extended conformation is reached through application of a penalty varying inversely with distance, coupled with a significantly larger penalty for each close contact.

Force Field. MD simulations used the OPLS-AA all-atom force field,[33−40] which has previously demonstrated reasonable accuracy for diverse chemical systems, including small molecules,[41] peptides,[42] and dendrimers.[43,44] Parameters were assigned to the system using parameter assignment routines implemented in the Silico script "namd_create_input". The majority of the OPLS-AA force field parameters were used without modification. However, in certain cases, we derived additional parameters.

Parameters for the Aryl Sulfonate Group. In the aryl sulfonate caps, three atom types had no pre-existing OPLS-AA parameters. These were the aromatic carbon atom bearing the sulfonate

* To whom correspondence should be addressed.
[†] Monash Institute of Pharmaceutical Sciences.
[‡] Verva Pharmaceuticals Ltd.

10.1021/ma802154e CCC: $40.75
Published on Web 03/10/2009

group and, within the sulfonate group, the sulfur atom and the three oxygen atoms. We adopted nonbonding parameters for the carbon atom from an aromatic carbon atom bearing a sulfonamide group. The Lennard-Jones σ and ε parameters for the sulfur and oxygen atoms were taken from sulfonamide and sulfone groups. We derived partial charges from those implemented in the MMFF94 force field[45−49] for the sulfur and oxygen atoms in sulfonate groups. We slightly decreased the positive charge on the sulfur atom and the negative charge on the oxygen, as we observed that MMFF94 charges on the carbon and hydrogen atoms in aromatic rings are also larger than the corresponding OPLS-AA charges. Bond, angle, dihedral, and improper dihedral parameters were adopted from existing parameters for aromatic sulfonamide groups. To establish that the charges adapted from the MMFF94 force field were appropriate, we calculated alternative charges using the restrained electrostatic potential (RESP) method.[50,51] The three sets of charges—Derived, MMFF94, and RESP—were compared by minimization of four crystal structures of aromatic sulfonates using the program XTALMIN, part of the TINKER package.[52] We compared the unit cell geometries of the minimized structures to those of the original unit cells, also carrying out an rms superposition of non-hydrogen atoms. The charges we derived gave comparable or better fits when compared to both unmodified MMFF94 charges and RESP charges and are suitable for use in MD simulations with the OPLS-AA force field.

Parameters for the Benzhydrylamide Group. A small number of atoms in the dendrimer core were also missing parameters. We took van der Waals parameters for these atoms from similar atom types present in the OPLS-AA force field. Partial charges were generated by slight modification of existing OPLS-AA parameters for similar atoms. Parameters for the benzhydrylamide group were validated using a crystal minimization of a molecule containing a benzhydrylamide group. After minimization, the unit cell geometry was comparable to the initial geometry. The values for our derived parameters, together with the results of the verification procedures, are provided as Supporting Information.

General Molecular Dynamics. Molecular dynamics simulations were performed with the program NAMD2.[53,54] Full periodic boundary conditions were used. Following a multiple time step protocol, forces from bonding interactions were evaluated every time step; those from van der Waals interactions and electrostatic interactions between atoms up to 12 Å apart were evaluated every second time step; and the remaining, long-range, electrostatic interactions were computed every four time steps using the particle-mesh Ewald (PME) algorithm[55,56] which has been shown to be accurate for molecular dynamics simulations.[57,58] The PME algorithm used a tolerance of 1×10^{-6} and an interpolation order of 4. The PME grid points were ∼1 Å apart. Unit cell sizes were chosen to ensure that the number of points along any dimension in the PME grid was composed of factors of 2, 3, and 5. Lennard-Jones potentials were used to model van der Waals interactions up to an interatomic distance of 10 Å. A switching function was used between 10 and 12 Å. Water molecules were modeled using the TIP3P model.[59] Counterions were modeled explicitly using standard OPLS-AA parameters. On a grid of 12 AMD Opteron CPUs (2.4−2.6 GHz), 10 ns of production MD of dendrimer **G4** (shown in Figure 1) completed in ∼8 days.

Compression and Simulated Annealing. Starmaker is designed to produce dendrimers in a highly extended conformation. This minimizes the risk of close contacts, and unphysical or undesirable structural defects such as *cis* amides and bonds passing through aromatic rings, arising during dendrimer construction. However, an extended PLL dendrimer is in an unfavorable conformation as well as requiring a larger solvent box and therefore a more computationally expensive simulation. To overcome this problem, we devised a simulation protocol which produces a compressed dendrimer and afterward uses simulated annealing to equilibrate the system.

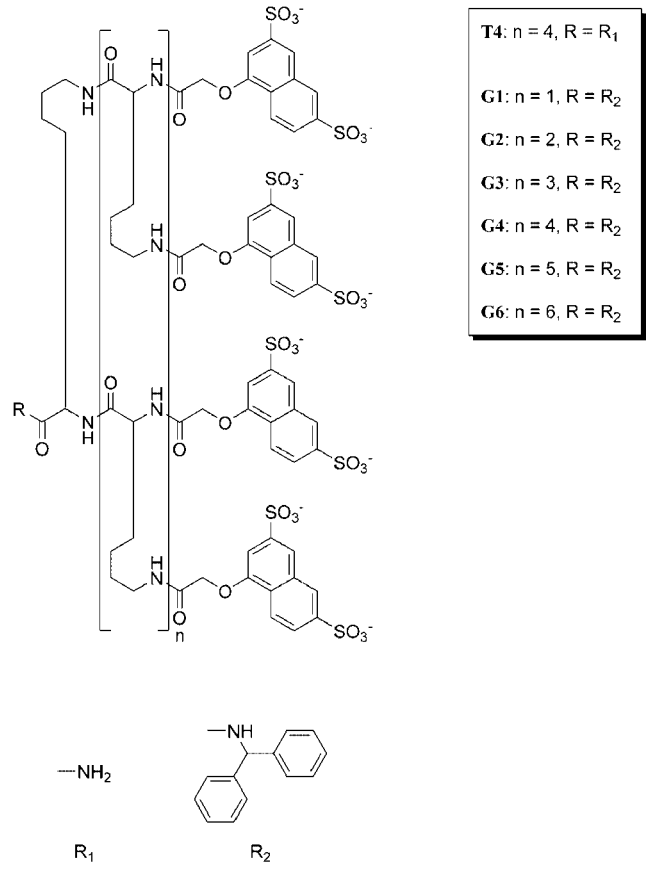

Figure 1. Structures of the test dendrimer **T4** and the dendrimers **G1** to **G6**.

As part of this protocol development process, we simulated the test dendrimer **T4**, which is similar to **G4**, lacking only the benzhydrylamide core (Figure 1). Three protocols were tested, as described in Table 1. Initially, we simulated **T4** for 5 ns under an NPT ensemble at $T = 300$ K as simulation **T4-E1**. We observed that when starting from an extended conformation, the solvent-accessible surface area of the dendrimer decreases slowly over the simulation, as the dendrimer gradually collapses. Using four 2.1 ns cycles of simulated annealing (simulation **T4-E2**), the dendrimer collapses much more quickly and produces results similar to those obtained from four cycles of simulated annealing, starting from a compressed conformation (simulation **T4-C**). We conclude that the compression protocol, used with simulated annealing, is appropriate for reaching equilibrium conformations and is better than a simulation beginning with an extended conformation, as it requires fewer solvent atoms and is therefore less computationally expensive. We have therefore used this protocol in our simulations.

Following this protocol, each dendrimer was compressed by applying conjugate-gradients energy minimization in vacuo for 30 000 steps, with artificial harmonic restraints of 9.00 kcal mol^{-1} $Å^{-2}$ applied from each atom to the initial position of an atom in the dendrimer's core. This was followed by a similar minimization without the harmonic restraints. In both these energy minimizations, we set atomic partial charges to zero, forced secondary amide bonds to adopt a *trans* geometry by adding a dihedral constraint of 1000 kcal mol^{-1} rad^{-2}, and did not apply periodic boundary conditions. Overall, this has the

effect of forcing the dendrimer into a compact, but chemically sensible, conformation. Following this, we added solvent molecules and counterions and carried out a third energy minimization. For this third minimization and all subsequent simulations, we applied full periodic boundary conditions, restored partial charges to their typical values and removed all constraints on rotation of amide bonds.

The equilibration protocol consisted of at least four cycles of simulated annealing with the periodic cell maintained at constant volume. In each of these cycles, the system was heated to 600 K over ~100 ps and cooled back to 300 K over ~2 ns. The final cycle of simulated annealing was followed by at least 2 ns of simulation using an NPT ensemble. During this simulation, the temperature was maintained at 300 K using the NAMD temperature coupling function, based on that implemented in X-PLOR.[60] The pressure was maintained at 1.013 25 bar using the pressure coupling method implemented in NAMD, a combination of the Nosé−Hoover constant pressure method[61] and Langevin piston fluctuation control.[62]

Production Molecular Dynamics. Once the equilibration protocol was finished, we simulated each dendrimer under the same NPT ensemble for a further 10 ns. During this time, we collected trajectory frames for analysis every 2 ps.

Visualization and Analysis. VMD[63] was used to view molecular dynamics output and to export structures from the trajectory as static files for further analysis. Molecule properties were calculated using Silico.[32] Images of molecules were rendered using PyMOL.[64]

Mean-squared radii of gyration[65] ($\langle R_g^2 \rangle$) were calculated as an ensemble average over the simulation. If **R** is the molecule's center of mass and $\mathbf{r}_i$ is the position of atom i

$$\langle R_g^2 \rangle = \left\langle \frac{1}{M} \sum_i^N m_i |\mathbf{r}_i - \mathbf{R}|^2 \right\rangle$$

The shape of the dendrimer can be quantified using the shape tensor, **G**, a diagonalizable matrix:

$$G_{uv} = \frac{1}{N} \sum_i^N (|r_{u,i} - R_u||r_{v,i} - R_v|)$$

$$\mathbf{G} = \begin{bmatrix} G_{xx} & G_{xy} & G_{xz} \\ G_{yx} & G_{yy} & G_{yz} \\ G_{zx} & G_{zy} & G_{zz} \end{bmatrix}$$

where u and v are any two of the three Cartesian axes: so, for example, $|r_{x,i} - R_x|$ is the component along the x-axis of the vector from the center of mass to the ith atom.

Diagonalization of the shape tensor gives three mutually orthogonal eigenvectors and three eigenvalues ($\lambda_1, \lambda_2, \lambda_3$). These are the directions and lengths, respectively, of the axes of the dendrimer's shape ellipsoid. Using these eigenvalues, the asphericity, δ, of the dendrimer is calculated, following the definition of Rudnick and Gaspari:[66]

$$\delta = 1 - 3\frac{\langle I_2 \rangle}{\langle I_1^2 \rangle}$$

where I_1 and I_2 are the first two invariants:

$$I_1 = \lambda_1 + \lambda_2 + \lambda_3$$
$$I_2 = \lambda_1\lambda_2 + \lambda_2\lambda_3 + \lambda_3\lambda_1$$

A value of $\delta = 0$ indicates that all atoms are evenly distributed on the surface of a sphere, while $\delta = 1$ if all atoms are in a straight line. A perfect circle has a shape anisotropy of $\delta = 0.25$.

Solvent-accessible surface areas were calculated using the program NACCESS,[67] which utilizes the method of Lee and Richards.[68] van der Waals radii for individual atoms were taken from the OPLS-AA force field. A spherical probe of radius 1.4 Å was used to trace the surface. Carbon atoms were defined as nonpolar; other non-hydrogen atoms were defined as polar. Hydrogen atoms were excluded from surface area calculations.

We calculated the density of atoms about a point as radial density profiles, similar to those of Kaplow et al.[69] The density $\rho_i(r)$ of a set of atoms i at a given radius r was calculated thus

$$\rho_i(r) = \frac{3N_i}{4\pi((r + \Delta r/2)^3 - (r - \Delta r/2)^3)}$$

where N_i is the number of atoms in the chosen set within the spherical shell defined by distances $r - \Delta r/2$ and $r + \Delta r/2$. To represent water distribution in and around the dendrimer, we have used the radial distribution function, $g_i(r)$, which is related to the radial density profile:

$$g_i(r) = \frac{\rho_i(r)}{[i]}$$

where $[i]$ is the concentration of species i in bulk solvent; for water, $[i] = 3.333 \times 10^{-2}$ Å^{-3}. Thus, $g_i(r) = 1$ in regions unaffected by the dendrimer.

To investigate the arrangement of caps around the dendrimer's center of mass, we developed a descriptor called the congregation coefficient, κ. In principle, the directional distribution of caps may range from lying along a single ray (perfect congregation) to even distribution on the surface of a sphere (perfect dispersion). To calculate the congregation coefficient of a set I, we first calculate a vector **A** from the dendrimer's center of mass **O** to the average position of the atoms in set I, along with a vector $\mathbf{U}_i$ from **O** to each atom i in the set I, which contains N_I atoms in total:

$$\mathbf{A} = \frac{1}{N_1} \sum_{i=1}^{N_1} \begin{bmatrix} x_i \\ y_i \\ z_i \end{bmatrix} - \mathbf{O}$$

$$\mathbf{U}_i = \begin{bmatrix} x_i \\ y_i \\ z_i \end{bmatrix} - \mathbf{O}$$

The ith atom's direction from the origin can now be determined as an angle θ_i relative to **A**:

Table 1. Composition of the Simulations of PLL Dendrimers up to the Sixth Generation[a]

simulation	N_{den}	N_{H_2O}	N_{Na^+}	N_{Cl^-}	N_{total}	box (Å)	V (Å^3)	caps
T4-E1, T4-E2	1551	48 618	64	0	50 233	78 × 84 × 78	511 056	32
T4-C	1551	13 617	64	0	15 232	59 × 56 × 50	165 200	32
G1	202	4 215	28	20	4 465	36 × 36 × 36	46 656	4
G2	398	8 226	55	39	8 718	45 × 45 × 45	91 125	8
G3	790	14 067	95	63	15 015	54 × 54 × 54	157 464	16
G4	1574	23 040	158	94	24 866	64 × 64 × 64	262 144	32
G5	3142	31 473	225	97	34 937	72 × 72 × 72	373 248	64
G6	6278	40 269	308	52	46 907	80 × 80 × 80	512 000	128

[a] N_{den}, N_{H_2O}, N_{Na^+}, N_{Cl^-}, and N_{total} are respectively the number of atoms in the dendrimer, of atoms in water molecules, of sodium ions, of chloride ions, and the total number of atoms. V is the initial periodic box volume. The "caps" column gives the number of caps in one dendrimer molecule.

$$\theta_i = \arccos\left(\frac{\mathbf{A}\cdot\mathbf{U}_i}{|\mathbf{A}||\mathbf{U}_i|}\right)$$

Space around **O** is divided into sectors by angle from **A** (Figure 2); the sector angle ϕ will ideally divide 180° evenly. The total number of sectors $S = 180°/\phi$. The first sector contains all atoms for which $\theta_i < \phi$; the second, all atoms for which $\phi \leq \theta_i < 2\phi$; and so on. The jth sector contains a fractional volume V_j of all space around **O** and is occupied by, as an ensemble average, N_j atoms belonging to set I; from these, we compute a normalized density, ρ_j, for this sector.

$$V_j = \frac{1}{2}(\cos((j-1)\phi) - \cos(j\phi))$$

$$\rho_j = \frac{N_j V_1}{N_I V_j}$$

The next step is to calculate the bias-uncorrected standard deviation σ of all values of ρ_j ($j = 1...S$). We also determine the perfect-congregation standard deviation σ_P. If all atoms in the set I were perfectly congregated, they would necessarily lie within the first sector; N_1 would therefore be equal to N_I, and ρ_1 would be 1, while ρ_j for all other sectors ($j = 2...S$) would be 0. σ_P is therefore calculated from s:

$$\sigma_P = \sqrt{\frac{1}{S} - \frac{1}{S^2}}$$

Division of σ by σ_P yields κ. κ may take values between 0 (perfect dispersion) and 1 (perfect congregation).

$$k = \frac{\sigma}{\sigma_P}$$

In this work, we used a sector angle of $\phi = 45°$. In this case, $S = 4$, and $\sigma_P = 0.4330$. We denote the congregation coefficient for this sector angle κ_{45}. A selection of theoretical distributions of caps and their congregation coefficients are shown in Figure 3.

Visual examination of the simulation trajectories of dendrimers containing naphthalene disulfonate caps revealed that the majority of these caps organize into stacks of various kinds (see below). We determined the extent of hydrophobic stacking by calculating the number of stacked naphthalene rings (at least one neighbor in a stack) and the number of sandwiched naphthalene rings (two neighbors in a stack). A naphthalene ring is defined as stacked if the distance between the center of the ring and the center of a neighboring naphthalene ring is less than 5 Å, as shown in Figure 4. Additionally, we used radial density profiles to show the proximity of caps to each other. To reduce the number of computations needed to determine the radial density profiles, instead of using all atoms in each cap, we used one of the bridgehead carbon atoms; this atom is indicated in Figure 4.

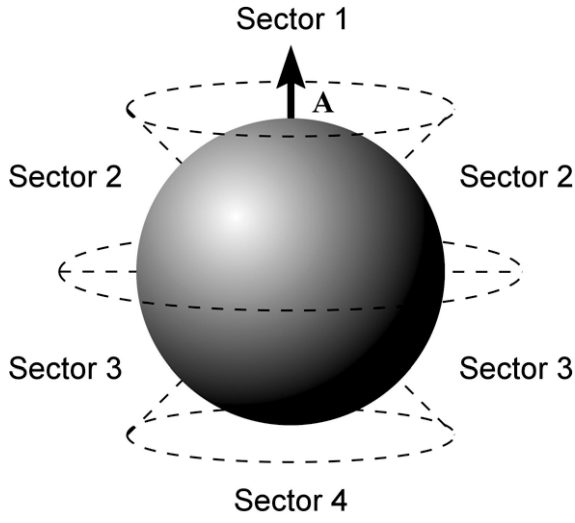

Figure 2. Division of space around the center of mass into spherical sectors, based on sector angles of 45° and starting from the vector **A**.

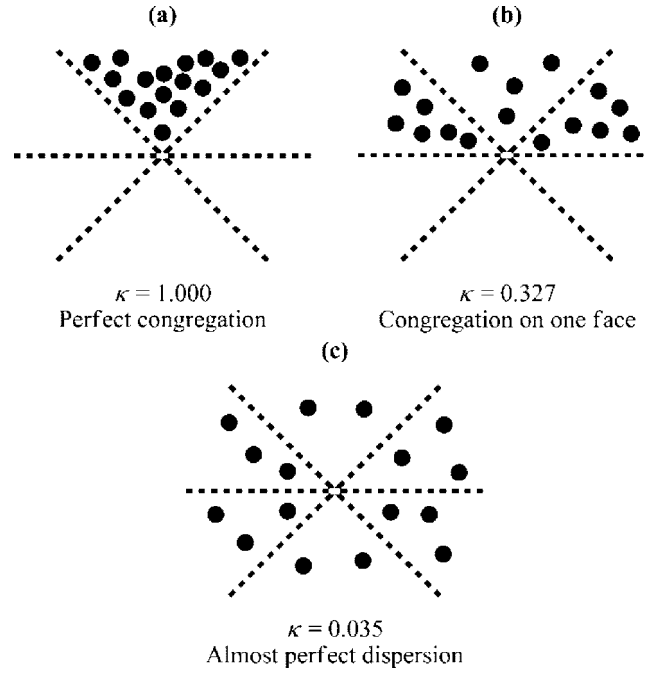

Figure 3. Some theoretical distributions of 16 caps about the center of mass and their congregation coefficients. (a) All caps are located in sector 1 (perfect congregation). (b) Caps are almost evenly spread throughout sectors 1 and 2, covering one face of the dendrimer. (c) Caps are almost evenly spread about all parts of the dendrimer. Apparent differences in cap concentration between populated sectors in (b) and (c) reflect a 2-dimensional representation of a sphere.

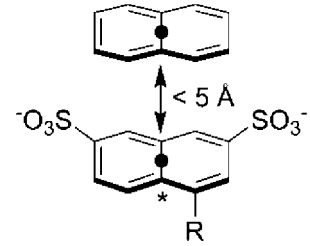

Figure 4. Criteria for the existence of a stack of naphthalene rings. The centers of the naphthalene rings are indicated as black circles (●), and the distance between the rings is calculated between these two points. The rings are stacked if this distance is less than 5 Å. The bridgehead atom in the cap which is used for radial density profiles is indicated in the bottom cap as *.

Results and Discussion

In this work we have investigated the structural characteristics of PLL dendrimers with naphthalene disulfonate caps. Using molecular dynamics simulations, we have modeled PLL dendrimers with a benzhydrylamide-(L-lysine) core and naphthalene disulfonate caps from the first to the sixth generation (**G1**−**G6**, Figure 1). We have studied the effect of generation number of gross molecular properties, such as size, shape, and exposed surface area and also investigated the behavior of the capping groups themselves. We have represented sulfonate groups as anions, consistent with their low pK_a, with sodium ions as

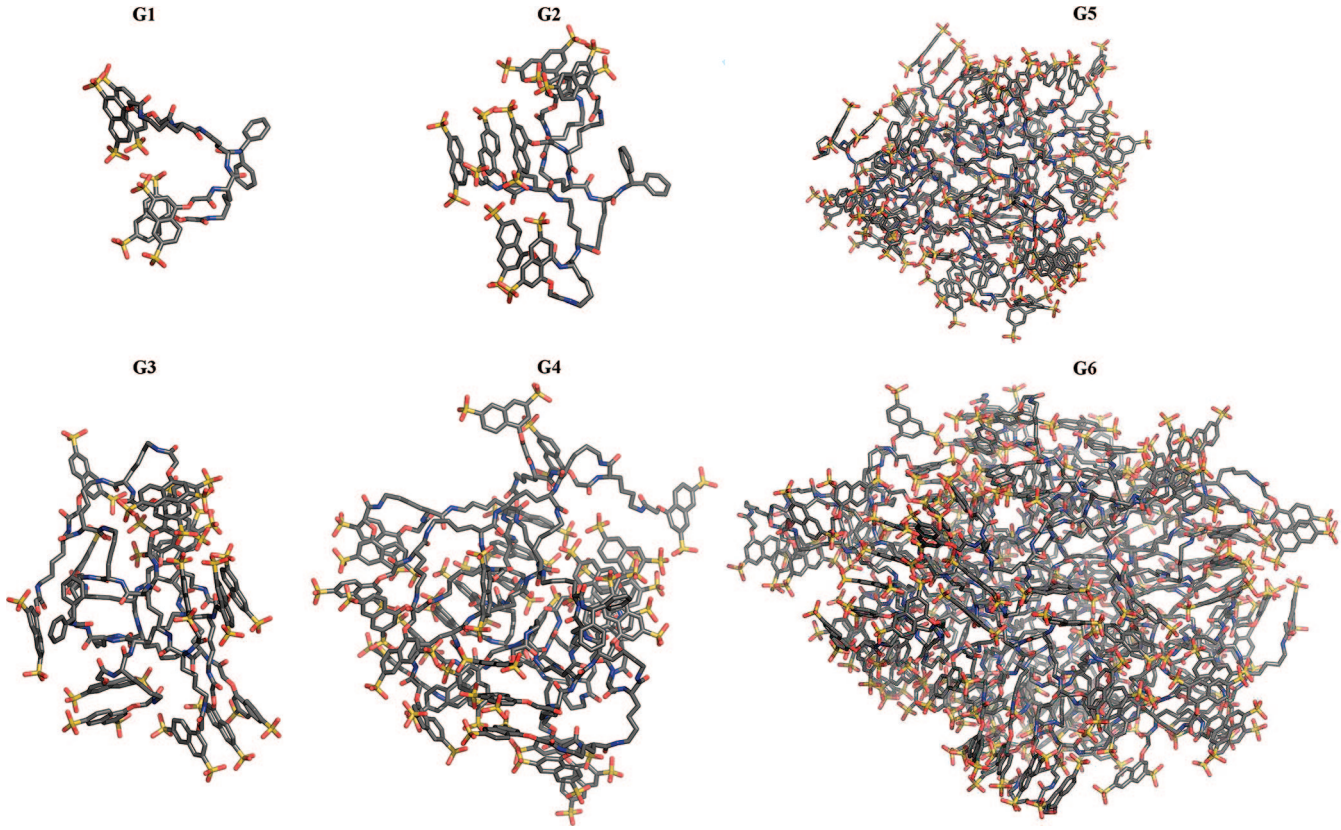

Figure 5. Final frames of the simulations of the dendrimers **G1** to **G4**. Solvent molecules, ions, and hydrogen atoms are not shown. Final frames of the simulations of the dendrimers **G5** and **G6**.

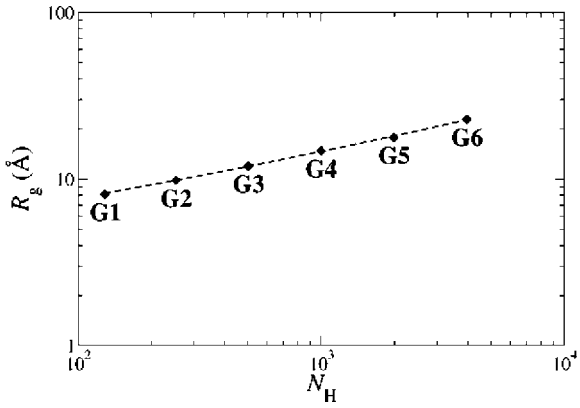

Figure 6. Mass-weighted radii of gyration of PLL dendrimers as a function of the number of heavy atoms. The generation number of each dendrimer is also shown.

Table 2. Asphericities of PLL Dendrimers G1−G6 and Their Comparison to Literature Values for PAMAM Dendrimers

		PAMAM		
generation	PLL	current authors	Paulo et al.[44]	Maiti et al.[78]
1	0.195		0.06	0.18
2	0.164		0.10	0.13
3	0.110		0.047	0.04
4	0.051	0.036 (protonated) 0.062 (neutral)	0.041	0.04
5	0.012		0.007	0.02
6	0.035			0.01

countercharges. To maintain a consistent ionic strength across the simulations, each dendrimer was simulated with Na^+ ions to a concentration of 1 M and enough Cl^- ions to provide overall electrical neutrality. The compositions of the simulated systems are shown in Table 1.

Whole-of-Molecule Properties. In the biological context for which PLL dendrimers have primarily been developed, dendrimer size is very important. In other dendrimer families, larger dendrimer size has been found to lead to greater in vitro cytotoxicity,[70,71] slower transportation from the bloodstream into tissues,[72] and more rapid clearance via the kidneys,[70] up to a limiting size. We have therefore sought to understand, by modeling, the relationship in PLL dendrimers between the generation number and properties such as size, shape, and intramolecular structure. The simulations show that, moving from low to high generations, a PLL dendrimer undergoes considerable structural change (Figure 5). All parts of dendrimer **G1** are open to the environment. As the generation number increases, a transition toward compact globules takes place and is essentially complete by **G5** and **G6**.

The radius of gyration provides an indication of the overall size of an approximately spherical molecule and can be determined experimentally using small-angle X-ray scattering (SAXS)[73,74] or small-angle neutron scattering (SANS).[75] The mean-squared radii of gyration of these dendrimers are shown in Figure 6 as a function of the number of heavy atoms (N_H). R_g scales as a power function of N_H: $R_g = 0.919N_H^{0.372} + 2.629$. This agrees well with the scaling of $R_g \propto N_H^{1/3}$, which is commonly reported for dendrimers in poor solvent[76−79] and is consistent with dense packing of atoms inside the dendrimer structure. There is no significant deviation from this trend for dendrimers up to **G6**.

Flexible dendrimers are known to adopt globular shapes in solution, with varying degrees of anisotropy; it has been previously observed that higher generations of dendrimers tend toward isotropic (spherical) shapes. We calculated asphericities for dendrimers **G1** to **G6** to determine whether this trend also

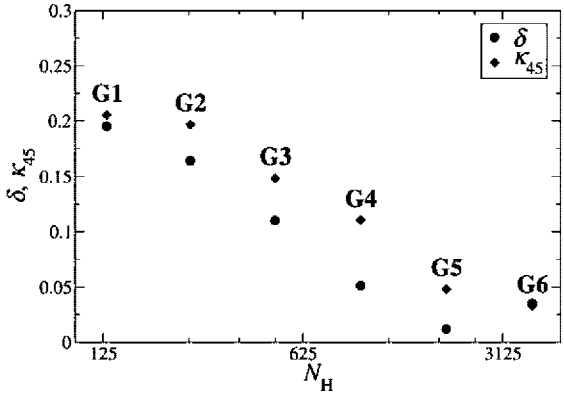

Figure 7. Asphericities (δ) and cap congregation coefficients (κ_{45}) of the PLL dendrimers **G1** to **G6** as a function of the number of heavy atoms.

occurs in PLL dendrimers. These results are shown and compared to the PAMAM dendrimers of Paulo et al.[44] and Maiti et al.[78] up to the sixth generation as well as our unpublished results concerning fourth-generation PAMAM dendrimers (see Table 2). PLL dendrimers are less spherical than Paulo's PAMAM dendrimers and comparable to those of Maiti and to our results. Asphericities as a function of number of heavy atoms are shown in Figure 7. The asphericity decreases as generation number increases, reaching a minimum at **G5** and increasing only slightly between **G5** and **G6**; these two dendrimers have essentially isotropic shapes. This is reflected in the shapes of the dendrimers (Figure 5). **G1** and **G2** are noticeably elongated; a transition to more or less isotropic shapes begins in **G3** and is complete by **G5** and **G6**.

An interesting possibility is that caps are spread unevenly about the surface of the dendrimer, whether due to asymmetry in the underlying framework or because of interactions between the caps themselves. An uneven distribution of caps will manifest itself as a high congregation coefficient. We have calculated congregation coefficients based on sectors of 45° (κ_{45}); these are shown in Figure 7 along with the asphericity. There is a significant degree of congregation in **G1**; as the generation number increases, the congregation coefficient decreases until, in the case of **G6**, the caps are almost perfectly dispersed about the dendrimer's center. This change largely occurs between **G2** and **G5**. The dendrimers **G3** and **G4** form a transition between the flexible, open lower generations, in which the dendrimer as a whole and its caps may be significantly asymmetric, and the densely packed higher generations in which the molecule is largely spherical and the caps to be more or less evenly distributed. The existence of significant congregation in the lower generations, especially **G1**, suggests that steric factors, rather than electronic effects such as electrostatic repulsion between sulfonate groups, are chiefly responsible for these morphological changes.

The properties of a molecule in solvent depend to a significant extent on the area of the molecule exposed to the solvent.[68] If the solvent-accessible surface area is very large, this indicates either a noticeably anisotropic shape or the presence of grooves (on the molecule's surface) or of voids (in the interior). In Figure 8, we show the solvent-accessible surface areas of the dendrimers as a function of generation number. The surface areas vary with the number of heavy atoms according to power laws, which are shown as dotted lines.

$$A_{\text{polar}} = 19.4 N_{\text{H}}^{0.797}$$

$$A_{\text{np}} = 13.5 N_{\text{H}}^{0.784}$$

$$A_{\text{total}} = 36.9 N_{\text{H}}^{0.775}$$

As expected, the majority of each dendrimer's solvent-accessible surface area is contributed by polar atoms. Dendrimers **G1** and **G2** have a relatively high proportion of their nonpolar surface accessible to solvent (showing a deviation from the fitted curves), which is expected given their visibly open conformations and inability to adopt a conformation in which most nonpolar atoms are buried in the interior. Consequently, the nonpolar component of the surface area is larger at low N_{H}. This characteristic of these low-generation dendrimers is not observed for **G3** and higher dendrimers, which have a dense structure in which hydrophobic regions are largely buried.

As a comparison, we consider a hypothetical family of spherical dendrimers with evenly distributed heavy atoms. Assuming that the internal atom density does not vary across generations, the solvent-accessible surface area also obeys a power law.

$$A_{\text{SAS}} \propto N_{\text{H}}^{2/3}$$

The surface areas of the simulated dendrimers scale more strongly with number of heavy atoms than expected, especially given the shift toward a spherical shape. The higher generations of dendrimers, rather than being smooth, have a heavily indented surface with deep grooves, e.g.,**G6** (Figure 9). This surface structure, while transient, affords scope for interaction sites.

The distribution of atoms within the dendrimers is shown using radial density profiles. These profiles allow us to determine

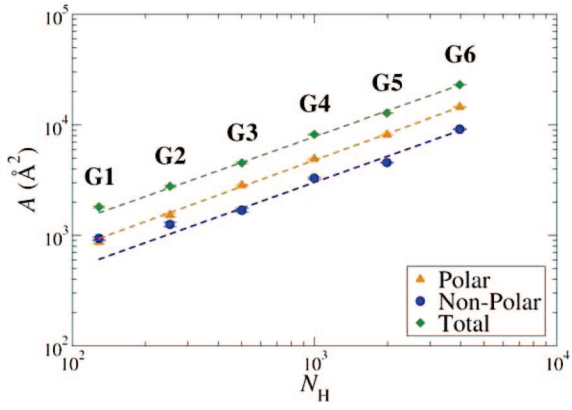

Figure 8. Solvent-accessible surface areas for polar atoms, nonpolar atoms, and all heavy atoms for the PLL dendrimers **G1** to **G6**, as a function of the number of heavy atoms. Fitted power functions are shown as dashed lines.

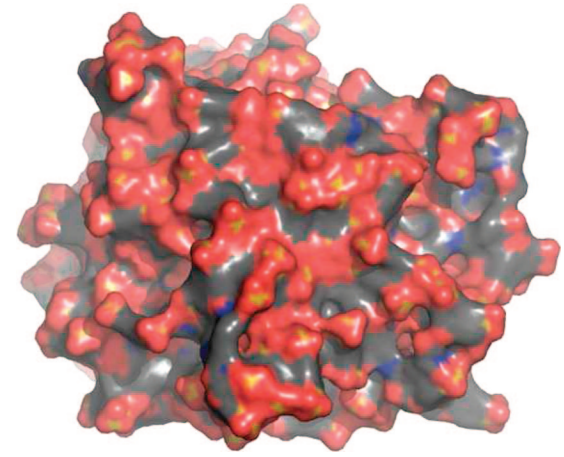

Figure 9. Dendrimer **G6** shown as a Connolly surface calculated using a probe radius of 1.4 Å.

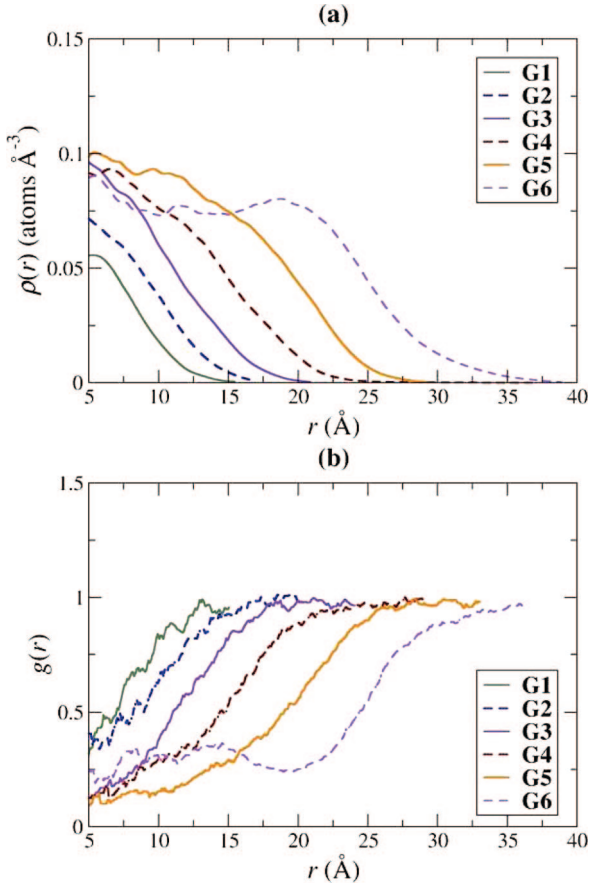

Figure 10. (a) Radial density profiles of dendrimer atoms about the dendrimer's center of mass and their variation with dendrimer generation. (b) Radial distribution functions of water molecules about the dendrimer's center of mass, based on the final structure only. Radial density profiles and distribution functions are shown as 4 Å moving averages.

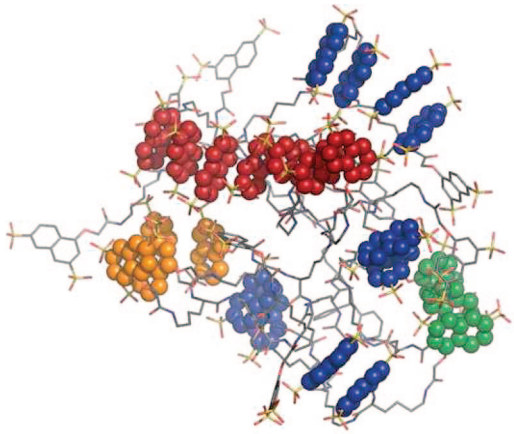

Figure 11. Naphthalene stacking in dendrimer **G4**. Stacked rings are shown as spheres; two-membered stacks are blue, a three-membered stack is green, a four-membered stack is orange, and a seven-membered stack is red.

whether or not voids are present on the interior of the dendrimer and whether PLL dendrimers are better described by a dense-core or dense-shell model. The radial density profiles of the dendrimers **G1** to **G6** are shown in Figure 10. The smaller dendrimers, up to **G4**, show a steady decrease in atom density after about 5 Å from the center of mass. We note, however, that the radial density profiles of these dendrimers are somewhat ambiguous because of their distortion from a spherical shape

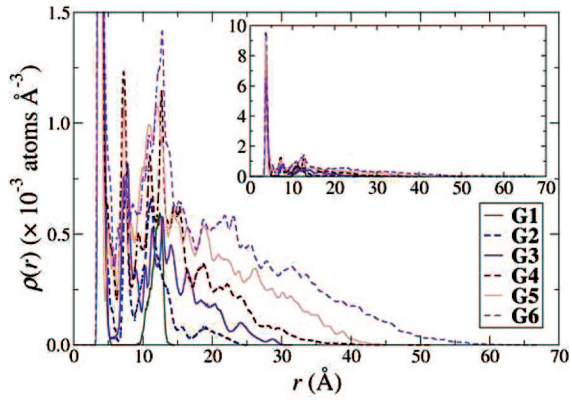

Figure 12. Mean radial density profiles of capping groups about capping groups and their variation with dendrimer generation. Axis units in the inset are as in the main graph.

(see Figure 7). Beginning at dendrimer **G5**, a "dense-core" region emerges; the inner parts of the dendrimer exhibit a relatively high and stable atom density. This core region extends to approximately 15 Å for **G5** and 20 Å for **G6**. This is almost half the maximum distance at which atoms are found and is approximately equal to the dendrimer's radius of gyration. At longer distances, a steady decrease in atom density takes place, similar to that observed in the lower generations. This decrease in atom density, along with earlier observations which suggest that the dendrimer's atoms are densely packed, is consistent with a dense-core model. Voids inside the dendrimer are occupied by water molecules, as shown by the increase in water concentration accompanying any decrease in dendrimer atom density. Up to **G5**, water levels increase toward the dendrimer's periphery. Interestingly, **G6** exhibits a local maximum in atom density at about 20 Å, where there are also relatively few water molecules; visual inspection of this dendrimer reveals that a dense peripheral region forms.

Unlike typical polypeptides, PLL dendrimers contain few hydrogen bonds, no more than one in three hydrogen-bond donors engaging in hydrogen bonding as determined by the criteria of McDonald and Thornton.[80] Ramachandran plots of the final frames of the simulations show that most of the lysine residues adopt extended conformations, as if for β-sheets, though in the higher generations, especially **G5** and **G6**, coiled lysine residues become more common, accounting for up to a third of all lysine residues (see Supporting Information).

Behavior of Caps. Inspection of dendrimer structures obtained by simulation immediately reveals significant interaction between the caps. The major mode of interaction is hydrophobic stacking. The stacking arrangement is most stable between caps which are forced by covalent bonds to be close together in space but also exists between other pairs of caps. We observed the formation of both short stacks (containing e.g. two naphthalene rings) and extended ladders, which may contain up to seven or eight naphthalene rings, as can be seen in the final frame of **G4** (Figure 11). It is common for the rings in these stacks to be offset from each other. This stacking interaction occurs in several other substances. Searching the Cambridge Structure Database,[81] we discovered at least 29 examples of compounds containing sulfonate-functionalized naphthalene rings which are stacked face-to-face when in a crystal lattice.

Regions of stacked naphthalene rings also contain large numbers of sodium ions, which associate strongly with the sulfonate groups. These sodium ions screen the electrostatic repulsion between sulfonate groups, allowing naphthalene rings to position themselves close to one another.

To determine the extent to which naphthalene rings associate with one another in these PLL dendrimers, we calculated radial density profiles of caps about caps (Figure 12). To simplify and speed up this calculation, we represented the location of each capping group by the carbon atom indicated in Figure 4. The widespread occurrence of stacking is shown by the large peak at $r = 4$ Å; smaller peaks at 8 and 12 Å indicate extended stacking arrangements. Beyond this peak at 12 Å, the radial density profile returns to a more conventional steady decrease in cap density.

The extent of stacking was also calculated. The criterion for a stacking interaction between two naphthalene rings is that the distance between their centers is less than 5 Å (Figure 4). More than 75% of caps are stacked, and in all dendrimers except **G1**, a significant proportion—more than 20%—of caps are sandwiched, as naphthalene rings organize into more extended stacks such as those depicted in Figure 11. In all generations, it is common for adjacent rings in stacks to be twisted and offset relative to one another.

Conclusions

We have simulated PLL dendrimers capped with naphthalene disulfonate groups, from the first to the sixth generation. We have developed an improved protocol for generating equilibrated dendrimers in solvent. PLL dendrimers display behavior which is typical of dendrimers in poor solvent and are comparable to other flexible dendrimers such as PAMAM, despite the differing symmetry. They demonstrate a gradual increase in size with generation number along with a shift from small molecule-like properties to more polymer-like properties. Dendrimers of the first and second generation are flexible and open, with nonpolar atoms mainly exposed to solvent. Dendrimers of the fifth and sixth generation adopt dense, largely spherical structures in which nonpolar atoms are largely buried, while the sixth-generation dendrimer possesses a dense shell. The surfaces of the higher-generation dendrimers have many recesses and protuberances. In the lower-generation dendrimers, caps are found somewhat congregated on the dendrimer's surface; caps are more evenly distributed about the dendrimer's center in the higher-generation dendrimers. Smaller, localized structural features within the dendrimer arise from the interaction between particular atoms or functional groups. A particularly prominent example of this in these PLL dendrimers is the stacking of the caps, which occurs in all generations and leads to considerable organization of the dendrimer's surface. This suggests the possibility of fine-tuning the dendrimer's surface structure, as well as chemical properties, by judicious choice of caps and raises the prospect of engineering dendrimer surfaces by taking advantage of cap−cap interactions.

Acknowledgment. This research was carried out in collaboration with Starpharma Pty Ltd. Financial support from the Australian Research Council is acknowledged. The authors thank the administrators of the Monash Sun Grid, the Victorian Partnership for Advanced Computing, and the Australian Partnership for Advanced Computing for supercomputer access.

Supporting Information Available: Parameters and parameter validation results for the benzhydrylamide core and the aromatic sulfonate group; instantaneous solvent-accessible surface areas of the test dendrimer under the three tested equilibration protocols; and graphs of simulation results including intramolecular hydrogen bonding, Ramachandran plots, and the extent of ring stacking; PDB format files for the final frames of the simulations of the dendrimers **G1** to **G6′**. This material is available free of charge via the Internet at http://pubs.acs.org.

References and Notes

(1) Denkewalter, R. G.; Kolc, J.; Lukasavage, W. J. Macromolecular highly branched homogeneous compound based on lysine units. U.S. Patent 4,289,872, 1981.
(2) Denkewalter, R. G.; Kolc, J. F.; Lukasavage, W. J. Macromolecular Highly Branched Homogeneous Compound. U.S. Patent 4,410,688, 1983.
(3) Tomalia, D. A.; Baker, H.; Dewald, J.; Hall, M.; Kallos, G.; Martin, S.; Roeck, J.; Ryder, J.; Smith, P. *Polym. J. (Tokyo, Jpn.)* **1985**, *17*, 117–132.
(4) Buhleier, E.; Wehner, W.; Vögtle, F. *Synthesis* **1978**, 155–158.
(5) Hawker, C.; Fréchet, J. M. J. *J. Chem. Soc., Chem. Commun.* **1990**, 1010–1013.
(6) Hawker, C. J.; Fréchet, J. M. J. *J. Am. Chem. Soc.* **1990**, *112*, 7638–7647.
(7) Hawker, C. J.; Wooley, K. L.; Fréchet, J. M. J. *J. Chem. Soc., Perkin Trans. 1* **1993**, 1287–1297.
(8) Choi, J. S.; Lee, E. J.; Choi, Y. H.; Jeong, Y. J.; Park, J. S. *Bioconjugate Chem.* **1999**, *10*, 62–65.
(9) Choi, J. S.; Joo, D. K.; Kim, C. H.; Kim, K.; Park, J. S. *J. Am. Chem. Soc.* **2000**, *122*, 474–480.
(10) Ohsaki, M.; Okuda, T.; Wada, A.; Hirayama, T.; Niidome, T.; Aoyagi, H. *Bioconjugate Chem.* **2002**, *13*, 510–517.
(11) Kester, M.; Stover, T.; Lowe, T.; Adair, J.; Kim, Y. S. Method and System for Systemic Delivery of Growth Arresting, Lipid-Derived Bioactive Compounds. Int. Patent WO 2004/096140, **2004**.
(12) Rana, T. M. RNA Interference Agents for Therapeutic Use. Int. Patent WO 2007/092182, **2007**.
(13) Tam, J. P. *Proc. Natl. Acad. Sci. U.S.A.* **1988**, *85*, 5409–5413.
(14) Tam, J. P. Multiple antigen peptide system. U.S. Patent 5,229,490, **1993**.
(15) Baigude, H.; Katsuraya, K.; Tokunaga, S.; Fujiwara, N.; Satoyama, M.; Magome, T.; Okuyama, K.; Borjihan, G.; Uryu, T. *J. Polym. Sci., Part A: Polym. Chem.* **2004**, *43*, 2195–2206.
(16) Baigude, H.; Katsuraya, K.; Okuyama, K.; Kariya, N.; Uryu, T. *Sen'i Gakkaishi* **2004**, *60*, 118–124.
(17) Roy, R.; Zanini, D.; Meunier, S. J.; Romanowska, A. *J. Chem. Soc., Chem. Commun.* **1993**, 1869–1872.
(18) Bourne, N.; Stanberry, L. R.; Kern, E. R.; Holan, G.; Matthews, B.; Bernstein, D. I. *Antimicrob. Agents Chemother.* **2000**, *44*, 2471–2474.
(19) Bernstein, D. I.; Stanberry, L. R.; Sacks, S.; Ayisi, N. K.; Gong, Y. H.; Ireland, J.; Mumper, R. J.; Holan, G.; Matthews, B.; McCarthy, T.; Bourne, N. *Antimicrob. Agents Chemother.* **2003**, *47*, 3784–3788.
(20) Matthews, B. R.; Holan, G.; Giannis, M. P. Agents for the Prevention and Treatment of Sexually Transmitted Diseases II. Int. Patent WO 2002/079298, **2002**.
(21) Matthews, B. R.; Holan, G.; Karellas, P.; Henderson, S. A.; O'Keefe, D. F. Agent for the Prevention and Treatment of Sexually Transmitted Diseases I. Int. Patent WO 2002/079299, **2002**.
(22) Krippner, G. Y.; Williams, C. C.; Kelly, B. D.; Henderson, S. A.; Wu, Z.; Razzino, P. Targeted Polylysine Dendrimer Therapeutic Agent. Int. Patent WO 2008/017125, **2008**.
(23) Caminade, A.-M.; Laurent, R.; Majoral, J.-P. *Adv. Drug Delivery Rev.* **2005**, *57*, 2130–2146.
(24) de Gennes, P. G.; Hervet, H. *J. Phys., Lett.* **1983**, *44*, L351−L360.
(25) Lescanec, R. L.; Muthukumar, M. *Macromolecules* **1990**, *23*, 2280–2288.
(26) Arai, T.; Ogawa, J.; Mouri, E.; Bhuiyan, M. P. I.; Nishino, N. *Macromolecules* **2006**, *39*, 1607–1613.
(27) Cattani-Scholz, A.; Renner, C.; Oesterhelt, D.; Moroder, L. *ChemBioChem* **2001**, *2*, 542–549.
(28) al-Jamal, K. T.; Sakthivel, T.; Florence, A. T. *Int. J. Pharm.* **2003**, *254*, 33–36.
(29) Boas, U.; Heegaard, P. M. H. *Chem. Soc. Rev.* **2004**, *33*, 43–63.
(30) Boas, U.; Christensen, J. B.; Heegaard, P. M. H. *Dendrimers in Medicine and Biotechnology: New Molecular Tools*; The Royal Society of Chemistry: Cambridge, UK, 2006.
(31) Rupp, R.; Rosenthal, S. L.; Stanberry, L. R. *Int. J. Nanomed.* **2007**, *2*, 561–566.
(32) Chalmers, D. K.; Roberts, B. P. Silico: A Perl Molecular Toolkit, http://silico.sourceforge.net. Accessed June 9, 2008.
(33) Jorgensen, W. L.; Maxwell, D. S.; Tirado-Rives, J. *J. Am. Chem. Soc.* **1996**, *118*, 11225–11236.
(34) Damm, W.; Frontera, A.; Tirado-Rives, J.; Jorgensen, W. L. *J. Comput. Chem.* **1997**, *18*, 1955–1970.
(35) McDonald, N. A.; Jorgensen, W. L. *J. Phys. Chem. B* **1998**, *102*, 8049–8059.
(36) Jorgensen, W. L.; McDonald, N. A. *THEOCHEM* **1998**, *424*, 145–155.
(37) Rizzo, R. C.; Jorgensen, W. L. *J. Am. Chem. Soc.* **1999**, *121*, 4827–4836.

(38) Price, M. L. P.; Ostrovsky, D.; Jorgensen, W. L. *J. Comput. Chem.* **2001**, *22*, 1340–1352.
(39) Watkins, E. K.; Jorgensen, W. L. *J. Phys. Chem. A* **2001**, *105*, 4118–4125.
(40) Kahn, K.; Bruice, T. C. *Bioorg. Med. Chem.* **2000**, *8*, 1881–1891.
(41) Martin, M. G. *Fluid Phase Equilib.* **2006**, *248*, 50–55.
(42) MacKerell, A. D., Jr. *Annu. Rep. Comput. Chem.* **2005**, *1*, 91–102.
(43) Peng, Y.; Kaminski, G. A. *J. Phys. Chem. B* **2005**, *109*, 15145–15149.
(44) Paulo, P. M. R.; Canongia Lopes, J. N.; Costa, S. M. B. *J. Phys. Chem. B* **2007**, *111*, 10651–10664.
(45) Halgren, T. A. *J. Comput. Chem.* **1996**, *17*, 490–519.
(46) Halgren, T. A. *J. Comput. Chem.* **1996**, *17*, 520–552.
(47) Halgren, T. A. *J. Comput. Chem.* **1996**, *17*, 553–586.
(48) Halgren, T. A. *J. Comput. Chem.* **1996**, *17*, 587–615.
(49) Halgren, T. A. *J. Comput. Chem.* **1996**, *17*, 616–641.
(50) Bayly, C. I.; Cleplak, P.; Cornell, W. D.; Kollman, P. A. *J. Phys. Chem.* **1993**, *97*, 10269–10280.
(51) Cornell, W. D.; Cleplak, P.; Bayly, C. I.; Kollman, P. A. *J. Am. Chem. Soc.* **1993**, *115*, 9620–9631.
(52) Ponder, J. TINKER Molecular Modeling Package, http://dasher.wustl.edu/tinker. Accessed February 12, 2008.
(53) Kalé, L.; Skeel, R.; Bhandarkar, M.; Brunner, R.; Gursoy, A.; Krawetz, N.; Phillips, J.; Shinozaki, A.; Varadarajan, K.; Schulten, K. *J. Comput. Phys.* **1999**, *151*, 283–312.
(54) Phillips, J. C.; Braun, R.; Wang, W.; Gumbart, J.; Tajkhorshid, E.; Villa, E.; Chipot, C.; Skeel, R. D.; Kalé, L.; Schulten, K. *J. Comput. Chem.* **2005**, *26*, 1781–1802.
(55) Darden, T.; York, D.; Pedersen, L. *J. Chem. Phys.* **1993**, *98*, 10089–10092.
(56) Essmann, U.; Perera, L.; Berkowitz, M. L.; Darden, T.; Lee, H.; Pedersen, L. G. *J. Chem. Phys.* **1995**, *103*, 8577–8593.
(57) Patra, M.; Karttunen, M.; Hyvönen, M. T.; Falck, E.; Lindqvist, P.; Vattulainen, I. *Biophys. J.* **2003**, *84*, 3636–3645.
(58) Patra, M.; Karttunen, M.; Hyvönen, M. T.; Falck, E.; Vattulainen, I. *J. Phys. Chem. B* **2004**, *108*, 4485–4494.
(59) Jorgensen, W. L.; Chandrasekhar, J.; Madura, J. D.; Impey, R. W.; Klein, M. L. *J. Chem. Phys.* **1983**, *79*, 926–935.
(60) Brünger, A. T. X-PLOR, Version 3.1; The Howard Hughes Medical Institute and Department of Molecular Biophysics and Biochemistry, Yale University, New Haven, CT, **1992**.
(61) Martyna, G. J.; Tobias, D. J.; Klein, M. L. *J. Chem. Phys.* **1994**, *101*, 4177–4189.
(62) Feller, S. E.; Zhang, Y.; Pastor, R. W.; Brooks, B. R. *J. Chem. Phys.* **1995**, *103*, 4613–4621.
(63) Humphrey, W.; Dalke, A.; Schulten, K. *J. Mol. Graphics* **1996**, *14*, 33–38.
(64) DeLano, W. L. The PyMOL Molecular Graphics System, http://pymol.sourceforge.net. Accessed June 1, 2008.
(65) Zwanzig, R. *J. Chem. Phys.* **1997**, *106*, 2824–2827.
(66) Rudnick, J.; Gaspari, G. *J. Phys. A: Math. Gen.* **1986**, *19*, L191−L193.
(67) Hubbard, S. J.; Thornton, J. M. NACCESS, London, UK, 1993.
(68) Lee, B.; Richards, F. M. *J. Mol. Biol.* **1971**, *55*, 379–400.
(69) Kaplow, R.; Strong, S. L.; Averbach, B. L. *Phys. Rev.* **1965**, *138*, A1336−A1345.
(70) Roberts, J. C.; Bhalgat, M. K.; Zera, R. T. *J. Biomed. Mater. Res.* **1996**, *30*, 53–65.
(71) Malik, N.; Wiwattanapatapee, R.; Klopsch, R.; Lorenz, K.; Frey, H.; Weener, J. W.; Meijer, E. W.; Paulus, W.; Duncan, R. *J. Controlled Release* **2000**, *65*, 133–148.
(72) El-Sayed, M.; Kiani, M. F.; Naimark, M. D.; Hikal, A. H.; Ghandehari, H. *Pharm. Res.* **2001**, *18*, 23–28.
(73) Prosa, T. J.; Bauer, B. J.; Amis, E. J.; Tomalia, D. A.; Scherrenberg, R. *J. Polym. Sci., Part B: Polym. Phys.* **1997**, *35*, 2913–2924.
(74) Omotowa, B. A.; Keefer, K. D.; Kirchmeier, R. L.; Shreeve, J. N. M. *J. Am. Chem. Soc.* **1999**, *121*, 11130–11138.
(75) Nisato, G.; Ivkov, R.; Amis, E. J. *Macromolecules* **1999**, *32*, 5895–5900.
(76) Sheng, Y.-J.; Jiang, S.; Tsao, H.-K. *Macromolecules* **2002**, *35*, 7865–7868.
(77) Giupponi, G.; Buzza, D. M. A. *J. Chem. Phys.* **2004**, *120*, 10290–10298.
(78) Maiti, P. K.; Çağin, T.; Wang, G.; Goddard, W. A., III. *Macromolecules* **2004**, *37*, 6236–6254.
(79) Suek, N. W.; Lamm, M. H. *Macromolecules* **2006**, *39*, 4247–4255.
(80) McDonald, I. K.; Thornton, J. M. *J. Mol. Biol.* **1994**, *238*, 777–793.
(81) Allen, F. H. *Acta Crystallogr., Sect. B: Struct. Sci.* **2002**, *B58*, 380–388.

MA802154E